Donor-Acceptor Index as a Descriptor for Electrolyte Design in High-Voltage Aqueous Batteries

Chuanyu Hou[a,b,c,e], *Miao Xie*[a,b,c,e], *Jianhui Wang*[a,b,c,d*]

[a]Research Center for Industries of the Future, Westlake University, Hangzhou 310030, China

[b]Key Laboratory of 3D Micro/Nano Fabrication and Characterization of Zhejiang Province, School of Engineering, Westlake University, Hangzhou 310030, China

[c]Institute of Advanced Technology, Westlake Institute for Advanced Study, Hangzhou 310024, Zhejiang, China

[d]Division of solar Energy Conversion and Catalysis at Westlake University, Zhejiang Baima Lake laboratory Co. Ltd., Hangzhou 310000, China

[e]These authors contributed equally to this work

***Corresponding author**

Email: wangjianhui@westlake.edu.cn

Abstract

Introducing organic molecules to anchor water can reduce water activity and expand the electrochemical stability window of aqueous electrolytes. However, there is a lack of reliable guidelines for screening suitable organic modulators. Through examining the effects of various organic molecules on the hydrogen bonding network of water, we found that the water-anchoring capabilities of organic modulators are positively correlated with their acceptor-donor index ($I_{A\text{-}D}$)—the sum of the products of donor and acceptor sites and their respective intensities. Furthermore, lithium metal titration-assisted differential electrochemical mass spectrometry (Li-DEMS) technique was developed to systematically investigate the charge-discharge behavior of three electrodes with different redox potentials ($Li_4Ti_5O_{12}$, V_2O_5, and Zn) in nonaqueous/aqueous hybrid electrolytes containing different organic modulators and salts. The contributions of the hydrogen evolution reaction (HER) and solid-electrolyte interphase (SEI) formation to irreversible capacity were decoupled. For all the electrodes studied, a higher $I_{A\text{-}D}$ value correlates with a smaller contribution of HER to irreversible capacities and higher initial and average Coulombic efficiencies. Notably, HER becomes the dominant contributor to irreversible capacity after the initial cycles. For the high-potential electrode (V_2O_5), electrochemical performance is primarily influenced by $I_{A\text{-}D}$, rather than SEI formation, while for the low-potential electrode ($Li_4Ti_5O_{12}$), both $I_{A\text{-}D}$ and SEI formation play significant roles in determining performance. These findings not only validate $I_{A\text{-}D}$ as a reliable descriptor for assessing the water-anchoring capabilities of organic modulators, but also establish a link between organic modulators, electrolyte solution structure, interphase reactions, and battery performances, providing valuable insights for the development of high-performance aqueous batteries.

1 Introduction

Aqueous electrolytes are nonflammable and moisture-resistant, the manufacturing of aqueous batteries does not require energy-intensive dry rooms. This offers distinct advantages in terms of cost, safety, and environmental sustainability when compared to nonaqueous batteries.[1-3] However, the long-standing challenge of the hydrogen evolution reaction (HER) at the cathode severely limits the operating voltage, energy density, and cycle life of aqueous batteries.[4] Increasing the salt

concentration can effectively widen the electrochemical stability window of aqueous electrolytes through the formation of unique solution structures and salt-derived, inorganic-rich solid electrolyte interphases (SEIs).[5,6] However, the high cost associated with increased salt concentrations hinders their widespread application.[7,8] Alternatively, the introduction of organic molecules to anchor water can also expand the electrochemical stability window of aqueous electrolytes by regulating the solution structure and SEI formation, without significantly increasing salt concentrations, making it a more feasible strategy.[9] Nevertheless, due to the vast number of organic compounds available, a reliable screening criterion for selecting suitable molecules is currently lacking.

Previous studies have linked the water-anchoring capabilities of organic molecules to various physicochemical parameters, yet most of these studies involved only 2~3 samples, leaving their general applicability unvalidated. Sulfolane (SL)[10] and trimethyl phosphate (TMP)[11] have been reported as efficient organic modulators for HER suppression, attributed to their high dielectric constants, which are thought to disrupt the hydrogen bonding network of water. However, other solvents with low dielectric constants, such as tetrahydrofuran (THF)[12] and Tetraglyme (G4)[13], have also demonstrated the ability to suppress HER. Furthermore, high donor number (DN) organic molecules, such as dimethyl sulfoxide (DMSO, DN = 29.8)[14] and N,N-dimethylacetamide (DMAC, DN = 27.8)[15], can partially replace water in the solvation shell, thereby suppressing HER. Interestingly, low-DN solvents, such as 1,4-dioxane (DN = 14.8)[16] and acetonitrile (DN = 14)[17], have also been shown to extend the cathodic potential limit due to their weak solvation ability, which results in the formation of anion-rich coordination. Additionally, amphiphilic molecules such as methylurea[18], urea[19], caprolactam[20], and glycerol[21] have demonstrated an excellent ability to reconstruct the hydrogen bonding network, thereby expanding the electrochemical stability window of aqueous electrolytes. However, no quantitative gauge has yet been established for measuring their effectiveness. Clearly, a reliable descriptor for screening efficient organic modulators has yet to be developed. Beyond regulating solution structure, which affects the thermodynamic stability of the electrolyte, organic modulators may also influence SEI formation, thereby affecting the kinetic stability of the electrolyte. However, previous studies have not distinguished between these two aspects, complicating the establishment of a clear structure-property relationship between the electrolyte solution structure and battery performance.

In our previous work, we identified that the solvent coordination ability in nonaqueous

electrolytes is primarily related to the DN value, rather than the dielectric constant or dipole moment of the solvent.[22] In aqueous electrolytes, the role of organic modulators is to anchor water, disrupting its hydrogen bonding network. Leveraging the DN rule of solvent coordination from nonaqueous systems and the amphiphilic donor-acceptor characteristics of water, we propose to evaluate the water-anchoring capability of organic modulators by considering both their donor and acceptor properties. By studying the effects of various organic modulators, including ethers, ketones, sulfoxides, phosphates, and amides, on the hydrogen bonding network of water, we establish a correlation between water-anchoring capability and the donor-acceptor index (I_{A-D}). To distinguish the effects of solution structure regulation and SEI formation on battery performance, we conducted a comparative study on the charge-discharge behavior of electrodes with different potentials (V_2O_5 vs. $Li_4Ti_5O_{12}$) in electrolytes containing different salts ($LiClO_4$ vs. LiTFSI). The operating voltage range of V_2O_5 (1.8~3.5 V vs. Li^+/Li) is significantly higher than that of $Li_4Ti_5O_{12}$ (1.4~1.8 V vs. Li^+/Li), and the charge-discharge behavior of the former is less reliant on SEI formation than that of the latter.[23] Similarly, the stable potential range of $LiClO_4$ salt (1.0~4.5 V vs. Li^+/Li) is significantly broader than that of LiTFSI (2.0~4.4 V vs. Li^+/Li), and $LiClO_4$-based electrolytes are less conducive to SEI formation on the anode as compared to LiTFSI-based ones.[24] Moreover, lithium metal titration-assisted differential electrochemical mass spectrometry (Li-DEMS) technique was developed to quantitatively analyze the contributions of HER and SEI formation to irreversible capacity during charge-discharge cycling. Ultimately, we establish a comprehensive structure-activity relationship encompassing "organic modulator characteristics – electrolyte solution structure regulation – interphase reactions decoupling – battery performance," providing new insights and valuable guidance for developing high-voltage aqueous batteries.

2 Results and discussion

2.1 I_{A-D} as Water-Anchoring Descriptor of Organic Modulators

To investigate the effect of organic modulators on the activity of water molecules, attenuated total reflectance-Fourier transform infrared (ATR-FTIR) spectroscopy was employed to analyze the hydrogen bonding network of water molecules in nonaqueous/aqueous hybrid solutions. As depicted in Figure 1a, the stretching vibration peak corresponding to the O−H bond of water molecules can be resolved to quantitatively demonstrate the hydrogen bonding configurations.[25] In pure water, a large

number of highly active water molecules interweave to form a hydrogen bonding network, with the infrared spectrum dominated by strong hydrogen bonding vibration peaks at low wavenumbers. In contrast, in hybrid solutions, the activity of water molecules is reduced due to the influence of organic modulators, leading to the formation of a significant content of non-hydrogen bond (Non-H bond) with vibration peaks at high wavenumbers. Consequently, the proportion of Non-H bond was utilized as a criterion to reflect the activity of water molecules in the hybrid solutions.

As shown in Table 1, organic modulators including ethers, esters, ketones, amides, and alkanes were selected and prepared into hybrid solutions with water at a molar ratio of 4:1 (named H_2O-4x). In the infrared spectra shown in Figure 1a, the strong hydrogen bonding infrared absorbance (DAA-OH, below 3100 cm^{-1}) is almost vanished in H_2O-4x hybrid solutions, indicating that the introduction of organic modulators effectively reduces the content of highly active water molecules. The proportion of Non-H bond configuration varying between 7.1% and 15.8% across the different solutions, which reflects considerable differences in the regulation abilities of various modulators on the activity of water molecules in the solutions. To establish a correlation between the activity of water molecules in the hybrid solutions and the physical parameters of the organic modulators, the proportions of Non-H bond against various physical parameters (dielectric constant (ε), molecular polarity (μ), and DN) was plotted in Figure 1b. The Pearson's coefficients in all three cases were less than 0.5, indicating a poor correlation between them. Therefore, the parameters (ε, μ, DN), which have been widely used to describe organic modulators in nonaqueous/aqueous hybrid solutions, do not demonstrate sufficient reliability for assessing the water-anchoring capabilities.

Leveraging the DN rule of solvent coordination from nonaqueous systems and the amphiphilic donor-acceptor characteristics of water, we consider both donor and acceptor properties of organic modulators to evaluate their water-anchoring capability. For an organic molecule, the donor site usually locates on the oxygen atom, whose lone pair of electrons participate in coordinating with the hydrogen atoms of water molecules. According to the FTIR results of ether-water solutions (Figure 1b), the proportion of Non-H bond is positively correlated with the number of oxygen atoms (G4 > G2 > THF). Moreover, comparing THF with AC, AC with a double-bonded oxygen atom exhibit stronger water-anchoring capability than THF because the double-bonded oxygen can interact with two hydrogen atoms simultaneously, whereas the single-bonded oxygen site only interacts with one hydrogen atom. Furthermore, due to the differences in the intensity of double-bonded oxygen atoms

of different functional groups (carbonyl oxygen, −C=O; sulfonyl oxygen, −S=O), organic molecules present different regulation abilities in aqueous solutions (DMSO > AC). Therefore, the water-anchoring capability of organic modulator is not only related to the strength of their donor sites but also to the number of their interaction sites. Similar interaction manner could be also applied on the acceptor properties of organic modulator. Therefore, we defined a donor-acceptor index ($I_{A\text{-}D}$) to be the sum of the products of donor and acceptor sites and their respective intensities, as expressed by the following formula:

$$I_{A\text{-}D} = DN * N_{DN} + AN * N_{AN}$$

Where DN and AN refer to the donor and acceptor numbers of the organic molecules, respectively, while N_{DN} and N_{AN} represent their corresponding intensity of donor and acceptor sites. The $I_{A\text{-}D}$ values of studied organic modulators were calculated and listed in Table 1. As shown in Figure 1b, the proportion of Non-H bond shows a positive linear relationship with $I_{A\text{-}D}$ (Pearson's coefficient r = 0.989), implying it a more reliable descriptor for assessing the water-anchoring capability of organic modulator. Moreover, we also analyzed the hydrogen bonding network of hybrid electrolytes with salts ($LiClO_4$ and LiTFSI) and found similar linear correlation between the proportion of Non-H bond and $I_{A\text{-}D}$ independent of salt type (Figure S1), confirming $I_{A\text{-}D}$ is an effective indicator for assessing the water-anchoring capability of organic modulator.

2.2 Correlation between $I_{A\text{-}D}$ and Electrochemical Stability Window of Electrolytes

To explore the relationship between the $I_{A\text{-}D}$ of organic modulators and the electrochemical window of aqueous electrolytes, linear sweep voltammetry (LSV) of a series of $LiClO_4$-H_2O-x (x = G2, DMSO, G4, TMP, TEP) hybrid electrolytes was measured. Due to the unfavorable properties of organics with low boiling points and high volatility for battery assembly, electrolytes prepared with AC and THF were not studied. As depicted in Figure 2a and 2b, the order of cathodic potential limit of $LiClO_4$-H_2O-x is consistent with that of onset potential of HER, implying that HER is a primary contributor to the reduction current within the aqueous electrolytes. More importantly, the order of cathodic potential limit of electrolytes can be correlated with the $I_{A\text{-}D}$ values of organic modulators. As the $I_{A\text{-}D}$ increases, the overpotential for the HER decreases. Specifically, the cathodic potential limit shifts from 2.31 V (versus Li/Li^+, in G2) to 1.64 V (versus Li/Li^+, in TEP), demonstrating a liner relationship with the $I_{A\text{-}D}$ (see Figure 2c). Moreover, the cyclic voltammetry tests of the electrolytes

revealed that, as depicted in Figure S2, the current density of electrolytes with high $I_{A\text{-}D}$ modulators (TMP, TEP) decreased by an order of magnitude in the second and third scans compared to the first scan. These results indicate that organic modulators with high $I_{A\text{-}D}$ can effectively anchor water molecules in the electrolyte.

2.3 Contribution Decoupling of HER and SEI to Irreversible Capacity

Organic modulators can influence both solution structure and SEI formation. However, previous studies have not distinguished between these two aspects, complicating the relationship between the electrolyte solution structure and battery performance. To distinguish these two effects, we conducted a comparative study on the charge-discharge behavior of V_2O_5//$LiMn_2O_4$ (LMO) and LTO//LMO batteries using hybrid electrolytes containing different salts ($LiClO_4$ vs. LiTFSI). The operating voltage range of V_2O_5 (1.8~3.5 V vs. Li^+/Li) is significantly higher than that of LTO (1.4~1.8 V vs. Li^+/Li), and the charge-discharge behavior of the former is less reliant on SEI formation than that of the latter. Similarly, the stable potential range of $LiClO_4$ salt (1.0~4.5 V vs. Li^+/Li) is significantly broader than that of LiTFSI (2.0~4.4 V vs. Li^+/Li), and $LiClO_4$-based electrolytes are less conducive to SEI formation on the anode as compared to LiTFSI-based ones. These design experiments allow the identification of the SEI role in battery performances.

HER and SEI formation are two factors contributing to irreversible capacity in high-voltage aqueous batteries, yet previous studies have not distinguished them either. Despite various techniques, such as in situ optical microscopy[26], gas chromatography[27], mass spectrometry[28], and X-ray CT[29], have been developed to detect hydrogen evolution during charge-discharge cycling. The produced side product of hydrogen is rarely quantitatively determined. In this work, we developed Li-DEMS technique to solve this issue. Utilizing the high-precise stoichiometric reaction of $2Li + 2H_2O = 2LiOH + H_2$, the side product of hydrogen gas detected by in situ DEMS can be quantitatively determined as shown in Figure 3a,b. Moreover, the hydrogen evolution signals of the V_2O_5//LMO and LTO//LMO full battery during the first and tenth cycles in the $LiClO_4$-H_2O-4x electrolytes were displayed in Figure S3 and S4. Subsequently, the contribution of HER and SEI formation to irreversible capacity can be calculated by the following equations.

The irreversible reaction capacity ($Q_{irreversible}$) is roughly contributed by two components: HER from water reduction (Q_{HER}), and irreversible capacity of the SEI formation (Q_{SEI}).

$$Q_{irreversible} = Q_{charge} - Q_{discharge} = Q_{HER} + Q_{SEI}$$

The total irreversible Coulombic efficiency (ICE_{total}) is defined as:

$$ICE_{total} = \frac{Q_{charge} - Q_{discharge}}{Q_{charge}}$$

The irreversible Coulombic efficiency caused by HER (ICE_{HER}) is defined as:

$$ICE_{HER} = \frac{Q_{HER}}{Q_{charge}}$$

The irreversible Coulombic efficiency caused by SEI (ICE_{SEI}) can be calculated:

$$ICE_{SEI} = ICE_{total} - ICE_{HER}$$

The contributions of ICE_{total} and ICE_{HER} of batteries using organic modulators with different $I_{A\text{-}D}$, fluorinated (LiTFSI) and nonfluorinated ($LiClO_4$)-based electrolytes are statistically analyzed and plotted in Figure 3c and Table S1. It can be seen that, for both $LiClO_4$ and LiTFSI, the ICE_{total} and ICE_{HER} of V_2O_5//LMO and LTO//LMO batteries decreases with the increase of the $I_{A\text{-}D}$ of organic modulators. During the first cycle, ICE_{HER} was considerably smaller than ICE_{total} in all batteries, which is due to the SEI formation caused by reduction reaction of organic modulators and lithium salts. In contrast, the ICE_{HER} was very close to ICE_{total} in all batteries at the tenth cycle, indicating that the electrode-electrolyte interface tended to stabilize and the reversibility of lithiation/delithiation process improved. Moreover, the percentage of the ICE_{HER} contribution to the ICE_{total} is plotted in Figure S5. It is indicated that the HER irreversible reaction accounted for the main part of the side reactions after initial cycles. On the one hand, compared to the V_2O_5//LMO battery, the ICE_{HER} contribution in the LTO//LMO battery was much higher, indicating that the low potential electrode suffers from more HER. On the other hand, compared to the aqueous electrolyte with low $I_{A\text{-}D}$ organic modulators, that with high $I_{A\text{-}D}$ organic modulators exhibit much reduced ICE_{HER}, thereby maintaining ICE_{total} at a lower level and achieving a high cycling stability.

2.4 Correlation between $I_{A\text{-}D}$ and Aqueous Li-ion Battery Performances

The correlation between the $I_{A\text{-}D}$ of organic modulators and the performance of aqueous lithium-ion batteries under long-cycle conditions was further presented. Figure 4a demonstrates the electrochemical performance and CE of V_2O_5//LMO full cells using $LiClO_4$-H_2O-4x and LiTFSI-H_2O-4x electrolytes at a 1C over 150 cycles. It is evident that electrolytes using organic modulators

with a high I_{A-D} always exhibit higher CE compared to those with a low I_{A-D}, along with better capacity retention and cycling stability. The same pattern was also observed in LTO//LMO full cells (Figure 4c). Furthermore, the initial and average CEs of V_2O_5//LMO batteries were presented in Figure 4b, which showed very close initial and average CEs using different electrolytes. This is because lithium salt anions (ClO_4^-, $TFSI^-$) produce less SEI on the high potential anode, which contributes less to the irreversible CE. Moreover, the average CE was found to be directly proportional to the I_{A-D} of the organic modulator. Specifically, the aqueous electrolyte using organic modulators with a high I_{A-D} enabled a high average CE exceeding 99%.

In contrast, LTO//LMO batteries with low redox potential anode showed significantly different charge-discharge behaviors using the hybrid electrolytes with different lithium salts. In particular, the initial and average CEs of batteries using LiTFSI were observed to be superior to those using $LiClO_4$, as depicted in Figure 4d. The enhancement is attributed to the reduction of $TFSI^-$ to form a solid SEI rich in inorganic substance, which effectively inhibits the HER side reaction. Furthermore, irrespective of the type of lithium salt utilized, a larger I_{A-D} always leads to a higher CE of battery. Notably, only the electrolytes that combined a fluoride-containing lithium salt with an organic modulator of high I_{A-D} were capable of elevating the average CE to exceed 99%. These findings underscore that battery performance is determined by both the I_{A-D} and SEI quality for low potential anodes, while the battery performance is dominated by the I_{A-D} independent of SEI for high-potential anodes.

2.5 Correlation between I_{A-D} and Aqueous Zinc Battery Performances

To verify the universal applicability of the I_{A-D} descriptor, a series of $Zn(ClO_4)_2$-H_2O-x electrolytes (x = G2, DMSO, G4, TMP, and TEP) were prepared and their performances were measured in Zn//Cu cells. It is worth noting that the selection of $Zn(ClO_4)_2$ salt over other fluoride-containing lithium salts was made to circumvent interference from fluoride-derived passivation layers, thereby facilitating a more precise analysis of the regulation capabilities. Furthermore, due to the relatively low solubility of $Zn(ClO_4)_2$ in the hybrid solvents, the molar ratio of the salt to water was carefully adjusted to 1:10. And the molar ratio of water to the organic modulators was kept as 1:4, the same with that in the lithium-ion system. The infrared spectra and the assignments of characteristic peaks for various electrolytes were compiled and presented in Figure S6. The analysis revealed that

an elevated I_{A-D} of the modulator correlates positively with an increased proportion of Non-H bond in the electrolytes, aligning with the observations discussed in foregoing sections.

CV curves of Zn//Cu cells using different hybrid electrolytes were shown in Figure 5a. Reversible Zn deposition and dissolution can be observed in all the studied electrolytes. The oxidation and reduction peak currents varied for different electrolytes, which is related to their differences in ionic conductivities and Zn-ion desolvation energy barriers. LSV in conjunction with Li-DEMS was employed to monitor the HER concurrent with the zinc deposition process in real-time, as depicted in Figure 5b. It was indicated that as the I_{A-D} of the organic modulator increased (G2 < DMSO < G4 < TMP < TEP), the onset potential for HER was progressively deferred accompanying with a continuous decrease in the peak intensity of generated hydrogen gas. As shown in Figure 5c, this produced hydrogen gas also present a linear correlation with I_{A-D}, confirming that the I_{A-D} descriptor for organic modulators remain applicable in aqueous zinc-ion system.

3 Conclusion

In summary, we introduced a donor-acceptor index (I_{A-D}) to evaluate the water-anchoring capabilities of organic molecules in aqueous solutions. This I_{A-D} shows a positive linear correlation with the proportion of Non-H bond and electrochemical stability window of nonaqueous/aqueous hybrid electrolytes. Moreover, we conducted a comparative study of the charge-discharge behavior of three electrodes with different redox potentials ($Li_4Ti_5O_{12}$, V_2O_5, and Zn) in nonaqueous/aqueous hybrid electrolytes containing different organic modulators (ethers, ketones, sulfoxides, phosphates, and amides) and salts ($LiClO_4$ and LiTFSI), and developed a Li-DEMS technique to decouple the contributions of HER and SEI formation to irreversible capacity of these aqueous batteries. The general findings are shown as follows: (1) For all the studied electrodes, as the I_{A-D} value increases, the irreversible capacity induced by HER is reduced and the initial and average CEs are enhanced. (2) For the high-potential electrode (V_2O_5), the electrochemical performance is primarily influenced by I_{A-D} independent of SEI formation. (3) For the low-potential electrode ($Li_4Ti_5O_{12}$), the electrochemical performance is determined by both I_{A-D} and SEI, particularly, good SEI favors good performances together with high I_{A-D} further improving performances. In addition, a positive correlation between I_{A-D} and electrochemical performance was also validated in aqueous zinc battery

performance. Consequently, our findings not only validate $I_{A\text{-}D}$ as a reliable descriptor for assessing the water-anchoring capabilities of organic modulators, but also establish a comprehensive structure-activity relationship encompassing "organic modulator characteristics – electrolyte solution structure regulation – interphase reactions decoupling – battery performance," providing new insights and valuable guidance for developing high-voltage aqueous batteries.

SUPPLEMENTAL INFORMATION

ACKNOWLEDGEMENTS

This work was supported by Research Center for Industries of the Future (RCIF) and Key Laboratory of 3D Micro/Nano Fabrication and Characterization of Zhejiang Province at Westlake university, Westlake Education Foundation, Zhejiang Baima Lake Laboratory Co. Ltd., and National Natural Science Foundation of China (Grant No. 21975207).

AUTHOR CONTRIBUTIONS

J.W. designed the experiments. C.H. carried out experiments. All authors contributed to the data analysis and manuscript preparation. J.W. conceived and led the project. C.H and M.X. contributed equally to this work.

DECLARARION OF INTERESTS

The authors declare no competing financial interest.

REFERENCES

(1) M. Armand, J.-M. Tarascon, *Nature* **2008**, 451, 652

(2) M. Li, C. Wang, Z. Chen, K. Xu, J. Lu, *Chemical reviews* **2020**, 120, 14 6783.

(3) Y. Liang, Y. Yao, *Nature Reviews Materials* **2023**, *8*, 2 109.

(4) H. Zhang, X. Liu, H. Li, I. Hasa, S. Passerini, *Angewandte Chemie International Edition* **2021**, *60*, 2 598.

(5) Y. Sui, X. Ji, *Angewandte Chemie International Edition* **2024**, *63*, 2 e202312585.

(6) L. Suo, D. Oh, Y. Lin, Z. Zhuo, O. Borodin, T. Gao, F. Wang, A. Kushima, Z. Wang, H.-C. Kim, et al., *Journal of the American Chemical Society* **2017**, *139*, 51 18670.

(7) D. Chao, S.-Z. Qiao, *Joule* **2020**, *4*, 9 1846.

(8) J. Xu, C. Wang, *Journal of The Electrochemical Society* **2022**, *169*, 3 030530.

(9) S. Chen, M. Zhang, P. Zou, B. Sun, S. Tao, *Energy & Environmental Science* **2022**, *15*, 5 1805.

(10) Y. Wang, T. Wang, D. Dong, J. Xie, Y. Guan, Y. Huang, J. Fan, Y.-C. Lu, *Matter* **2022**, *5*, 1 162.

(11) Q. Li, C. Yang, J. Zhang, X. Ji, J. Xu, X. He, L. Chen, S. Hou, J. Uddin, D. Addison, et al., *Angewandte Chemie International Edition* **2022**, *61*, 49 e202214126.

(12) C. Zhang, B. Chen, Q. Chen, Y. Liu, X. Kong, L. Suo, J. Lu, H. Pan, *Advanced Materials* **2024**, *36*, 40 2405913.

(13) Y. Shang, N. Chen, Y. Li, S. Chen, J. Lai, Y. Huang, W. Qu, F. Wu, R. Chen, *Advanced Materials* **2020**, *32*, 40 2004017.

(14) Q. Nian, X. Zhang, Y. Feng, S. Liu, T. Sun, S. Zheng, X. Ren, Z. Tao, D. Zhang, J. Chen, *ACS Energy Letters* **2021**, *6*, 6 2174.

(15) P. Jiang, J. Zhang, T. Zhan, K. Zhang, W. Jian, D. Ruan, *ACS Materials Letters* **2024**, *6*, 4 1216.

(16) Q. Nian, W. Zhu, S. Zheng, S. Chen, B.-Q. Xiong, Z. Wang, X. Wu, Z. Tao, X. Ren, *ACS Applied Materials & Interfaces* **2021**, *13*, 43 51048.

(17) Z. Ma, J. Chen, J. Vatamanu, O. Borodin, D. Bedrov, X. Zhou, W. Zhang, W. Li, K. Xu, L. Xing, *Energy Storage Materials* **2022**, *45* 903.

(18) R. Lin, C. Ke, J. Chen, S. Liu, J. Wang, *Joule* **2022**, *6*, 2 399.

(19) J. Xu, X. Ji, J. Zhang, C. Yang, P. Wang, S. Liu, K. Ludwig, F. Chen, P. Kofinas, C. Wang, *Nature Energy* **2022**, *7*, 2 186.

(20) L. Zhou, S. Tian, X. Du, T. Liu, H. Zhang, J. Zhang, S. Hu, Z. Chen, J. Zhang, G. Cui, *ACS Energy Letters* **2022**, *8*, 1 40.

(21) Z. Huang, T. Wang, X. Li, H. Cui, G. Liang, Q. Yang, Z. Chen, A. Chen, Y. Guo, J. Fan, et al., *Advanced Materials* **2022**, *34*, 4 2106180.

(22) J. Chen, H. Zhang, M. Fang, C. Ke, S. Liu, J. Wang, *ACS Energy Letters* **2023**, *8*, 4 1723.

(23) X. Hou, L. Zhang, N. Gogoi, K. Edstrom, E. J. Berg, *Small* **2024**, *20*, 23 2308577.

(24) R. Lin, J. Chen, C. Ke, S. Liu, J. Wang, *Journal of Energy Chemistry* **2023**, *77* 180.

(25) C. Choe, J. Lademann, M. E. Darvin, *Analyst* **2016**, *141*, 22 6329.

(26) Y. Shang, S. Chen, N. Chen, Y. Li, J. Lai, Y. Ma, J. Chen, F. Wu, R. Chen, *Energy & Environmental Science* **2022**, 15, 6 2653.

(27) C.-C. Kao, C. Ye, J. Hao, J. Shan, H. Li, S.-Z. Qiao, *ACS nano* **2023**, 17, 4 3948.

(28) J. Xie, Z. Liang, Y.-C. Lu, *Nature materials* **2020**, 19, 9 1006.

(29) J. Scharf, L. Yin, C. Redquest, R. Liu, X. L. Quinn, J. Ortega, X. Wei, J. Wang, J.-M. Doux, Y. S. Meng, *Advanced Energy Materials* **2021**, 11, 33 2101327.

Table 1. Information about the studied organic solvents: Donor numbers (DN), Acceptor numbers (AN), Dielectric Constants (ε), Dipole Moments (μ) and Donor-Acceptor Index (I_{A-D}).

Label	Organic solvents	DN	AN	ε	μ	I_{A-D}
1	 Tetrahydrofuran (**THF**)	20.00	8.00	7.60	1.63	28.00
2	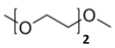 Diglyme (**G2**)	19.50	9.90	7.20	1.92	68.40
3	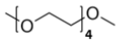 Tetraglyme (**G4**)	16.60	10.5	7.70	2.44	83.00
4	 Dimethyl sulfoxide (**DMSO**)	29.8	19.3	47.20	4.10	78.90
5	 Acetone (**AC**)	17.00	12.50	20.70	2.88	46.50
6	 Trimethyl phosphate (**TMP**)	23.00	16.30	21.60	2.82	131.30
7	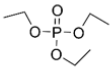 Triethyl phosphate (**TEP**)	23.40	20.40	13.00	2.86	137.40

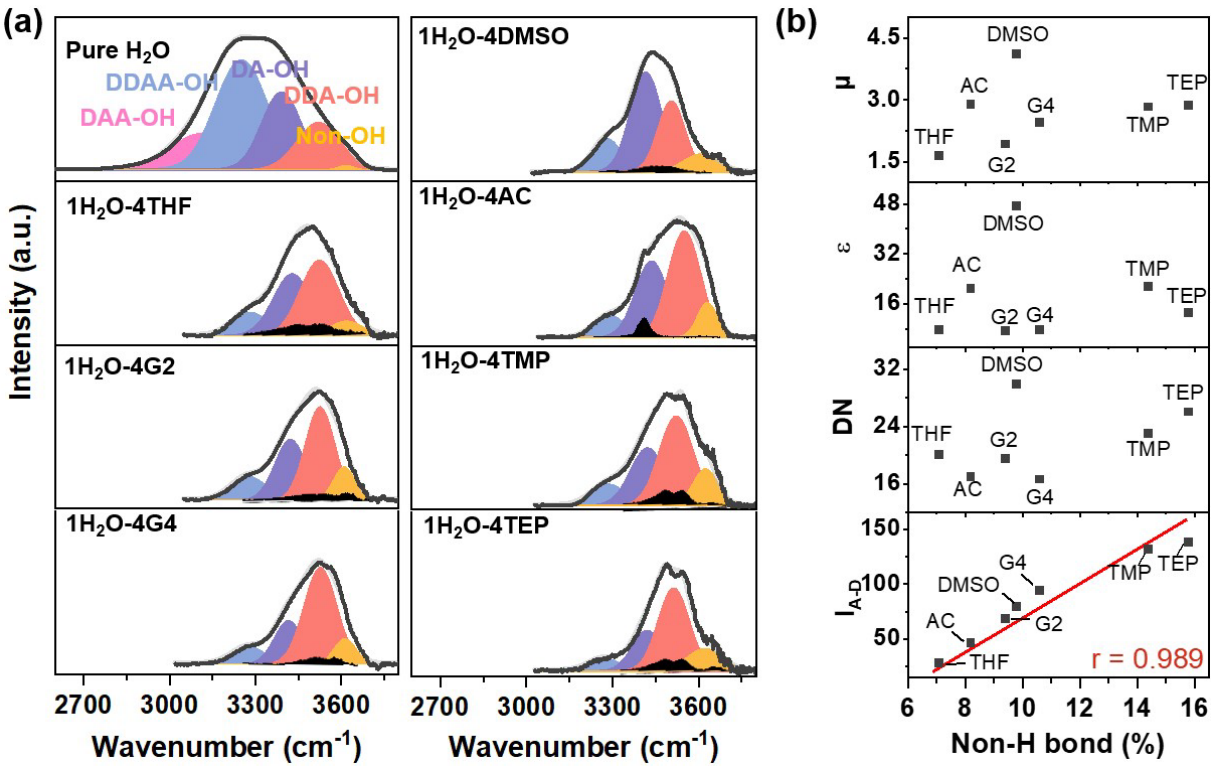

Figure 1. Correlation of hydrogen bonding structure with various physical parameters of organic modulators. (a) Quantitative analysis of infrared O-H stretching peaks in pure H_2O and various organic/water solutions ($1H_2O$-4x). (b) Correlation of dipole moments (μ), dielectric constants (ε), donor numbers (DN), donor-acceptor index (I_{A-D}) with Non-H bond of $1H_2O$-4x solutions. Pearson's r reflects the degree of linear correlation between the two variables.

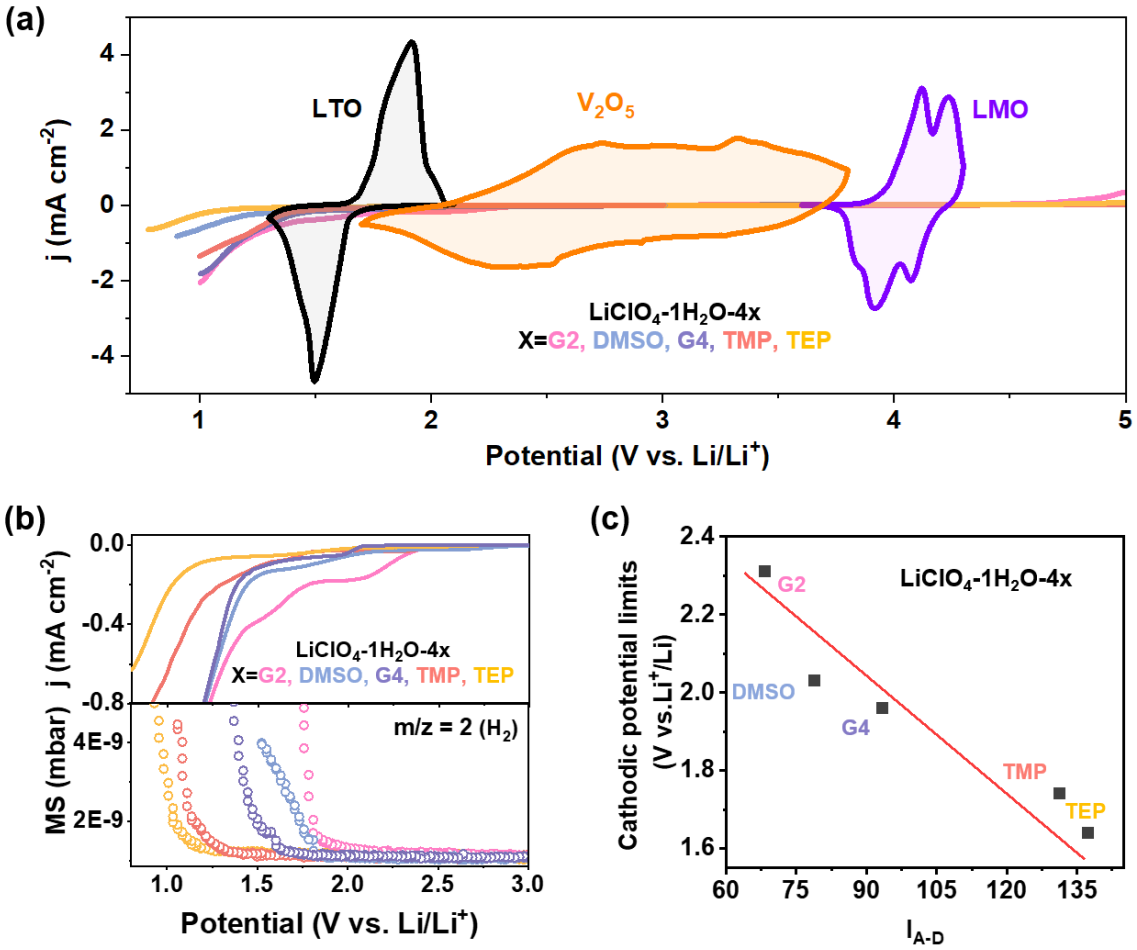

Figure 2. Correlation of I_{A-D} with electrochemical stability window of various nonaqueous/aqueous hybrid electrolytes. (a) Cathodic and anodic LSV curves on Ti foil as work electrode in the $LiClO_4$−H_2O−x electrolytes. Typical CV curves of LTO, V_2O_5 and LMO electrodes were also presented. (b) Cathodic LSV curves in $LiClO_4$−H_2O−x electrolytes (upper panel) accompanying with H_2 evolutions detected by in situ DEMS (lower panel). (c) Correlation of I_{A-D} with the cathodic potential limits of $LiClO_4$−H_2O−x electrolytes. X= G2, DMSO, G4, TMP and TEP. The LSV scan rat is 5 mV s^{-1}.

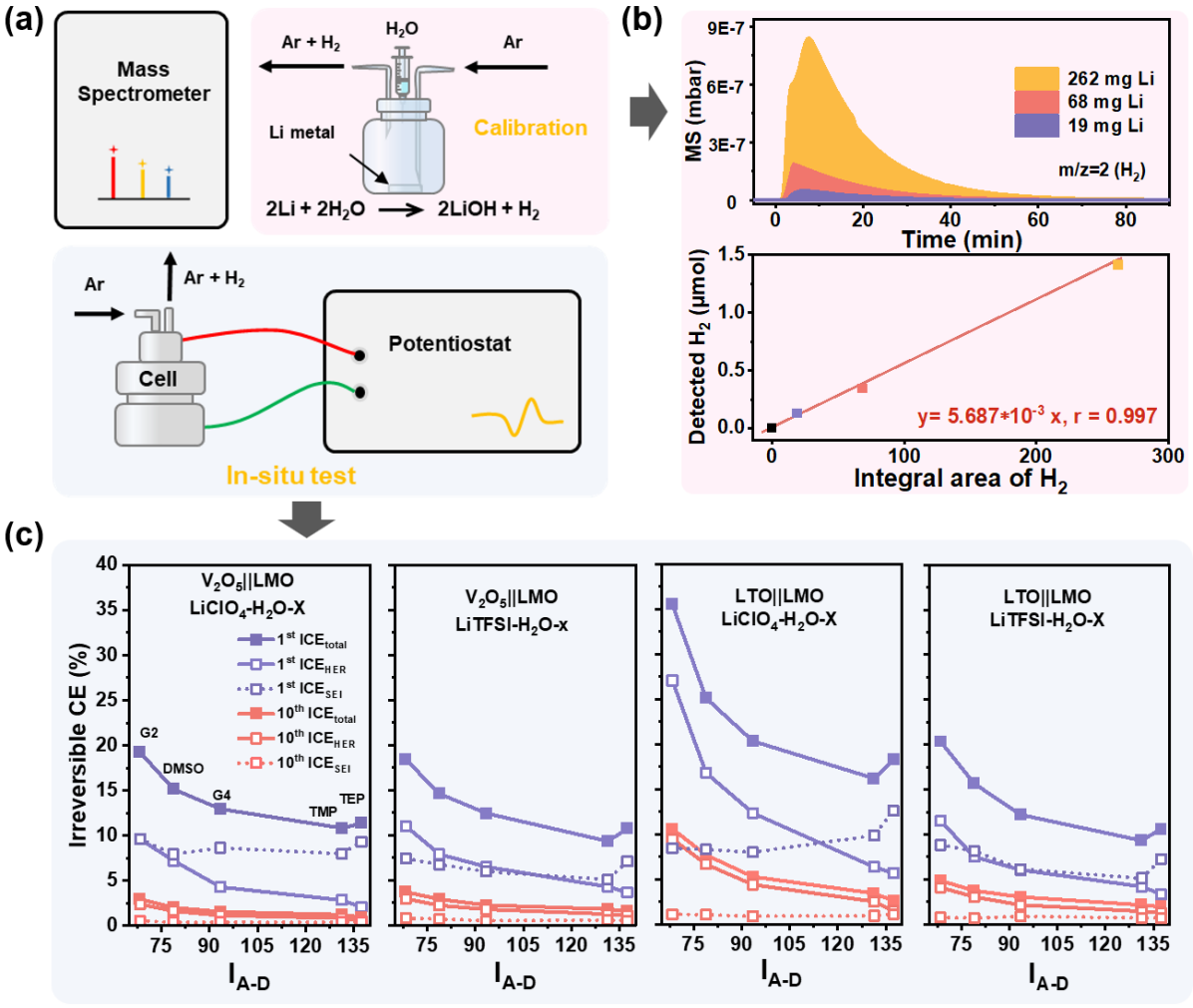

Figure 3. Quantitative analysis of HER contribution to irreversible capacity via lithium metal titration-assisted differential electrochemical mass spectrometry (Li-DEMS). (a) Schematic illustration of Li-DEMS technique. (b) Calibration of H_2 MS signals using Li metal titration. The good linear relationship between the integrated area of detected H_2 and the calculated molar mass of H_2 confirms it a reliable quantitative analytic method. (c) Correlation of ICE_{total} and ICE_{HER} contributions in different batteries with I_{A-D} of organic modulators. ICE_{SEI} = ICE_{total} - ICE_{HER}.

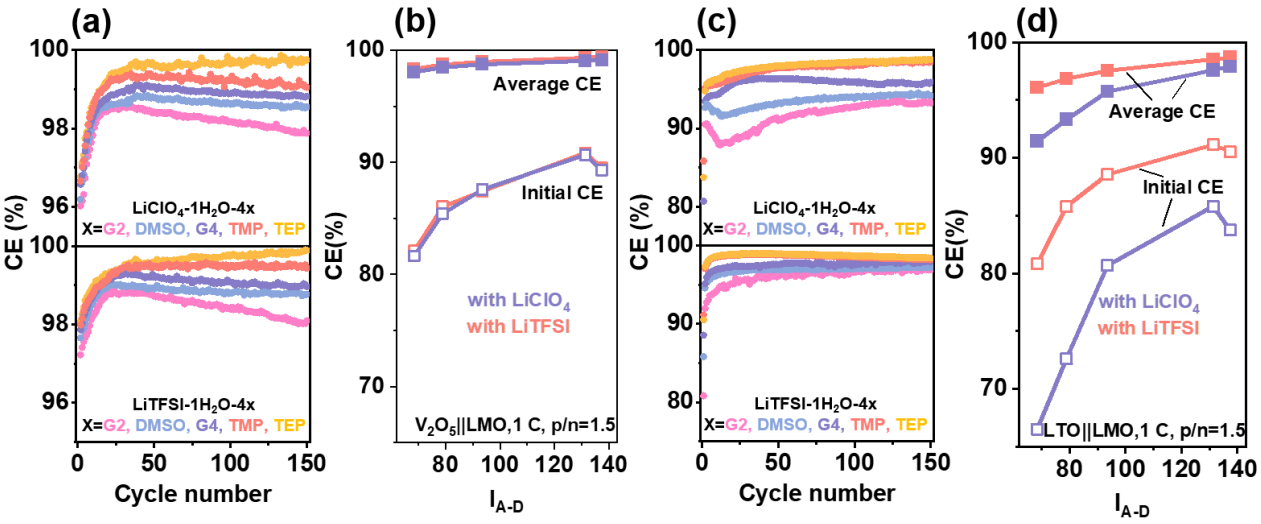

Figure 4. Correlation of I_{A-D} with CEs of different batteries in various nonaqueous/aqueous hybrid electrolytes. (a) CEs of V_2O_5//LMO full cells using LiTFSI-H_2O-X and $LiClO_4$-H_2O-X electrolytes. (b) Correlation of initial and average CEs of V_2O_5//LMO full cells with I_{A-D} of organic modulators. (c) CEs of LTO//LMO full cells using LiTFSI-H_2O-X and $LiClO_4$-H_2O-X electrolytes. (d) Correlation of initial and average CEs of LTO//LMO full cells with I_{A-D} of organic modulators. X= G2, DMSO, G4, TMP and TEP.

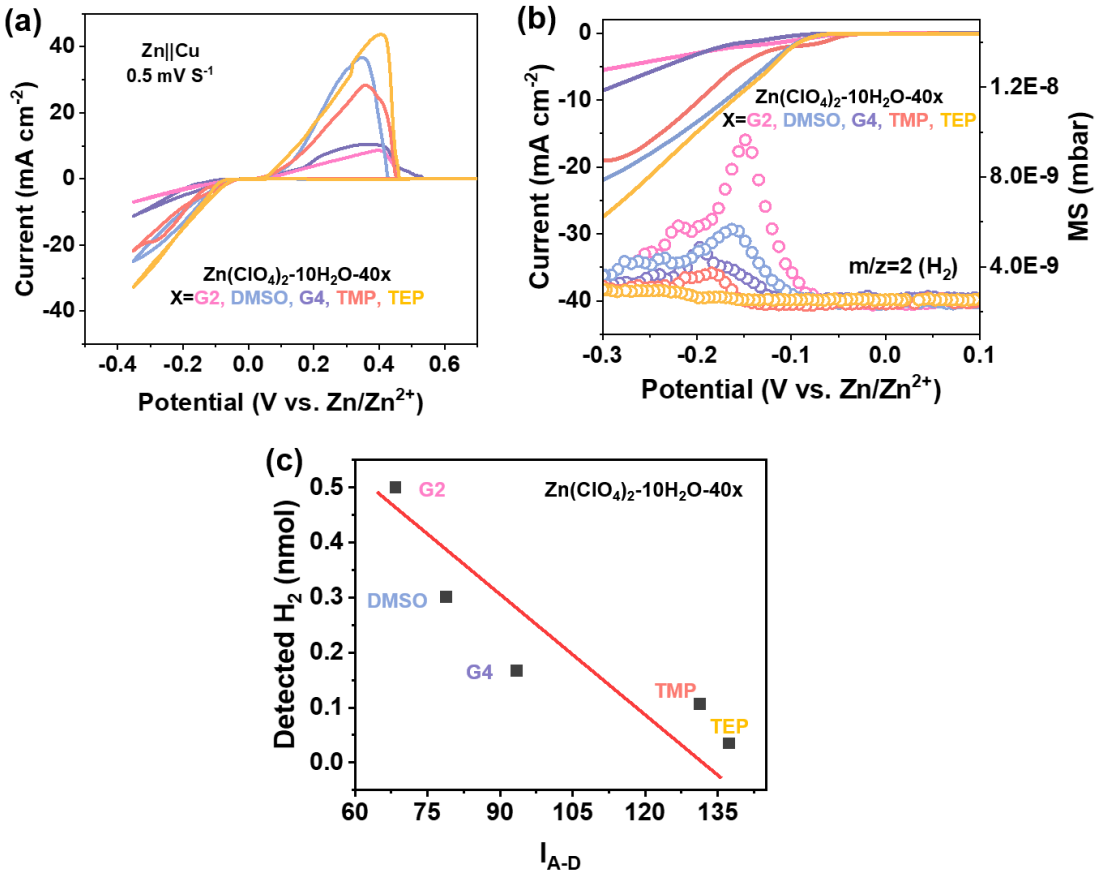

Figure 5. Correlation of I_{A-D} with H_2 evolution on Zn electrode in various nonaqueous/aqueous hybrid electrolytes. (a) CV curves of Zn//Cu cells in the $Zn(ClO_4)_2$-H_2O-X electrolytes. (b) H_2 evolution in the $Zn(ClO_4)_2$-H_2O-X electrolytes during cathodic LSV scans. (c) Correlation of I_{A-D} with H_2 evolution detected during the cathodic LSV scans. X= G2, DMSO, G4, TMP and TEP. The scan rates of CV and LSV are 0.5 mV s^{-1}.

Supplementary Information for

Donor-Acceptor Index as a Descriptor for Electrolyte Design in High-Voltage Aqueous Batteries

Chuanyu Hou[a,b,c,e], *Miao Xie*[a,b,c,e], *Jianhui Wang*[a,b,c,d*]

[a]Research Center for Industries of the Future, Westlake University, Hangzhou 310030, China

[b]Key Laboratory of 3D Micro/Nano Fabrication and Characterization of Zhejiang Province, School of Engineering, Westlake University, Hangzhou 310030, China

[c]Institute of Advanced Technology, Westlake Institute for Advanced Study, Hangzhou 310024, Zhejiang, China

[d]Division of solar Energy Conversion and Catalysis at Westlake University, Zhejiang Baima Lake laboratory Co. Ltd., Hangzhou 310000, China

[e]These authors contributed equally to this work

***Corresponding author**

Email: wangjianhui@westlake.edu.cn

Experimental

Solution Preparation

Lithium perchlorate ($LiClO_4$), lithium bis(trifluoromethanesulphony)imide (LiTFSI), triethyl phosphate (TEP), trimethyl phosphate (TMP), dimethyl sulfoxide (DMSO), tetraglyme (G4), diglyme (G2), tetrahydrofuran (THF), and acetone (AC) were purchased from Dodo Chem in Suzhou. Ultrapure water was obtained from Adamas. The water/organic hybrid solutions were prepared in a 1:4 molar ratio by mixing H_2O with organic solvents such as TEP, TMP, THF, AC, DMSO, G2, and G4 thoroughly. Electrolytes, such as Li−H_2O−4TEP, Li−H_2O−4TMP, Li−H_2O−4G2, Li−H_2O−4G4, and Li−H_2O−4DMSO, were prepared at a molar ratio of $LiClO_4$: water: organic = 1:1:4 for electrochemical testing. Similarly, the zinc hybrid electrolytes were prepared using $Zn(ClO_4)_2 \cdot 6H_2O$ obtained from Adamas, ultrapure water, and organic solvents in a 1:10:40 molar ratio.

Electrode Preparation

V_2O_5, $Li_4Ti_5O_{12}$, $LiMn_2O_4$, activated carbon, and polyvinylidene fluoride (PVDF) were purchased from Guangdong Canrd New Energy Technology Co., Ltd. All these electrode materials were used directly without any surface coating. The active materials (V_2O_5, $Li_4Ti_5O_{12}$, $LiMn_2O_4$, and activated carbon), acetylene black, and PVDF were thoroughly mixed with N-methyl pyrrolidone (NMP, Suzhou DodoChem) at a mass ratio of 90:5:5 to prepare the electrode slurries. Subsequently, they were uniformly cast onto titanium foils (10 μm thick, Chengnuo Metal) using an automatic coater (Hefei Kejing Materials Technology Co., Ltd., MSK-AFA-I). Finally, the coated electrodes were dried under vacuum at 120°C for more than 8 hours, calendered, and cut into discs with a diameter of 11.3 μm.

Electrochemical Tests

For three-electrode cell (Swagelok-type cell), linear sweep voltammetry (LSV) and cyclic voltammetry (CV) were utilized to test the electrochemical stability window of electrolytes. The active carbon and Ag/AgCl (3.239 V vs. Li/Li^+) were used as the counter and reference electrode, respectively. The LSV and CV tests were conducted on an electrochemical workstation (BioLogic, MPG-2) with a titanium foil as the working electrode. The scan rate is 5 mV s^{-1}. The 2032 coin cells were assembled using $LiMn_2O_4$ cathode, V_2O_5 or $Li_4Ti_5O_{12}$ anodes, and glass fiber (Whatman, GF/A) separator. Titanium foil was added between the electrode and the battery shell for protection. The full cells were subjected to a constant current charge-discharge cycling on a battery test system (Shenzhen

Neware, CT-4008).

Characterizations

ATR-FTIR measurements. The hydrogen bonding network of water molecules in the solutions was characterized by an attenuated total reflectance-Fourier transform infrared spectrometer (ATR-FTIR, ThermoFisher, iS50), with spectral recordings of 16 scans and a resolution of 4 cm^{-1}.

Li-DEMS measurements. The hydrogen evolution during cycling was detected by a quadrupole mass spectrometer (QAS 100, Shanghai Linglu) using a specially designed Swagelok cell. The quantitative analysis of the detected hydrogen gas was conducted based on the high-precise stoichiometric reaction of lithium metal with water ($2Li + 2H_2O \rightarrow 2LiOH + H_2$). Before Li-DEMS measurement, the Swagelok cell was flushed with argon gas for 1 hour to remove air in the cell.

Figures & Tables

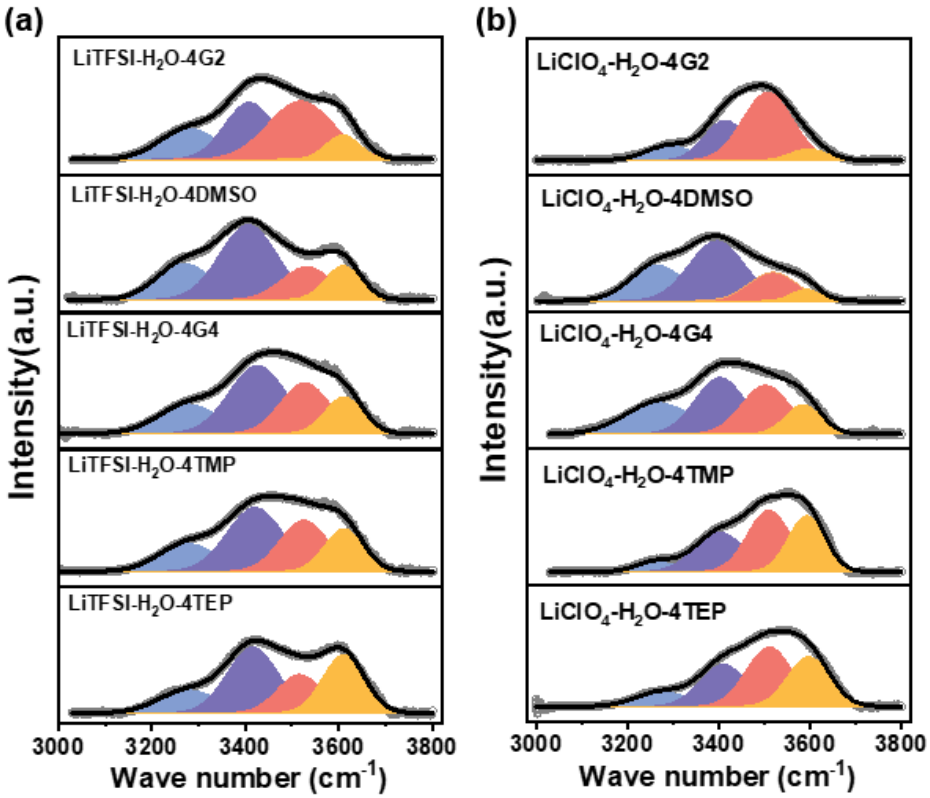

Figure S1. Quantitative analysis of infrared O-H stretching peaks in the hybrid electrolytes of (a) LiTFSI-H_2O-x and (b) $LiClO_4$-H_2O-x.

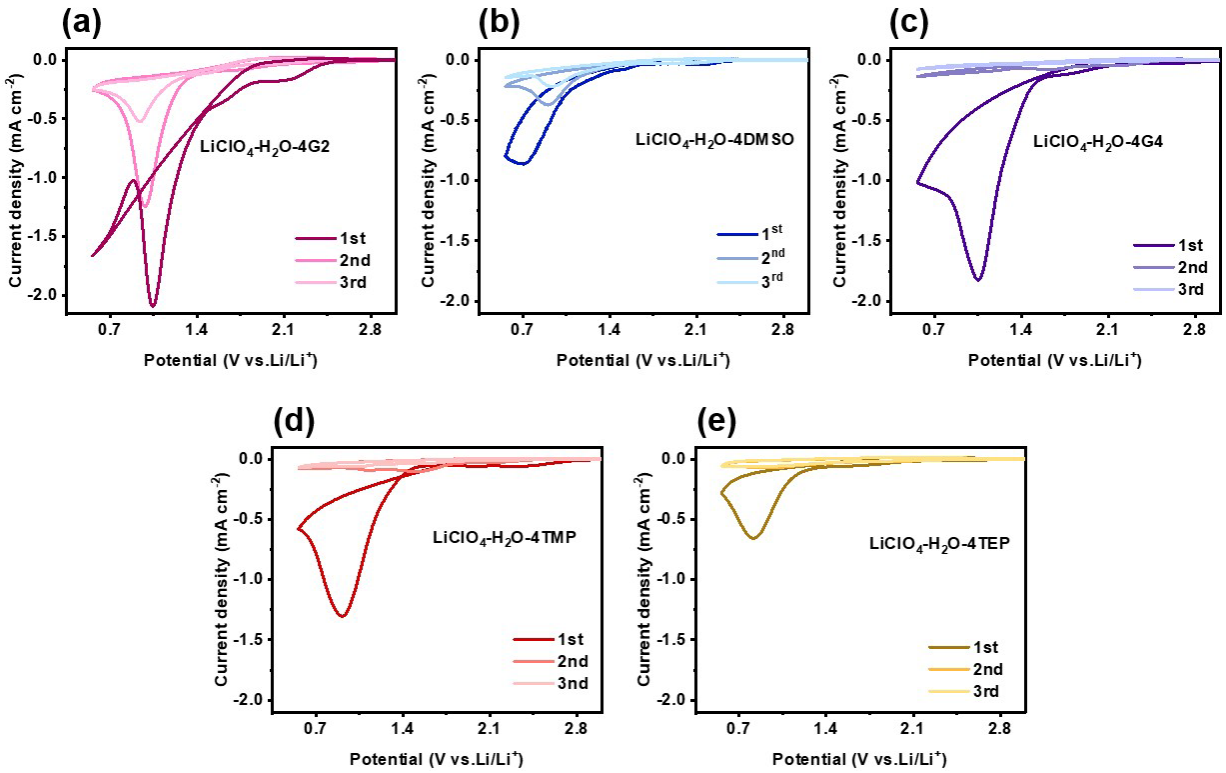

Figure S2. CV curves of Ti electrode in the $LiClO_4$-H_2O-x electrolytes during the first three cycles.

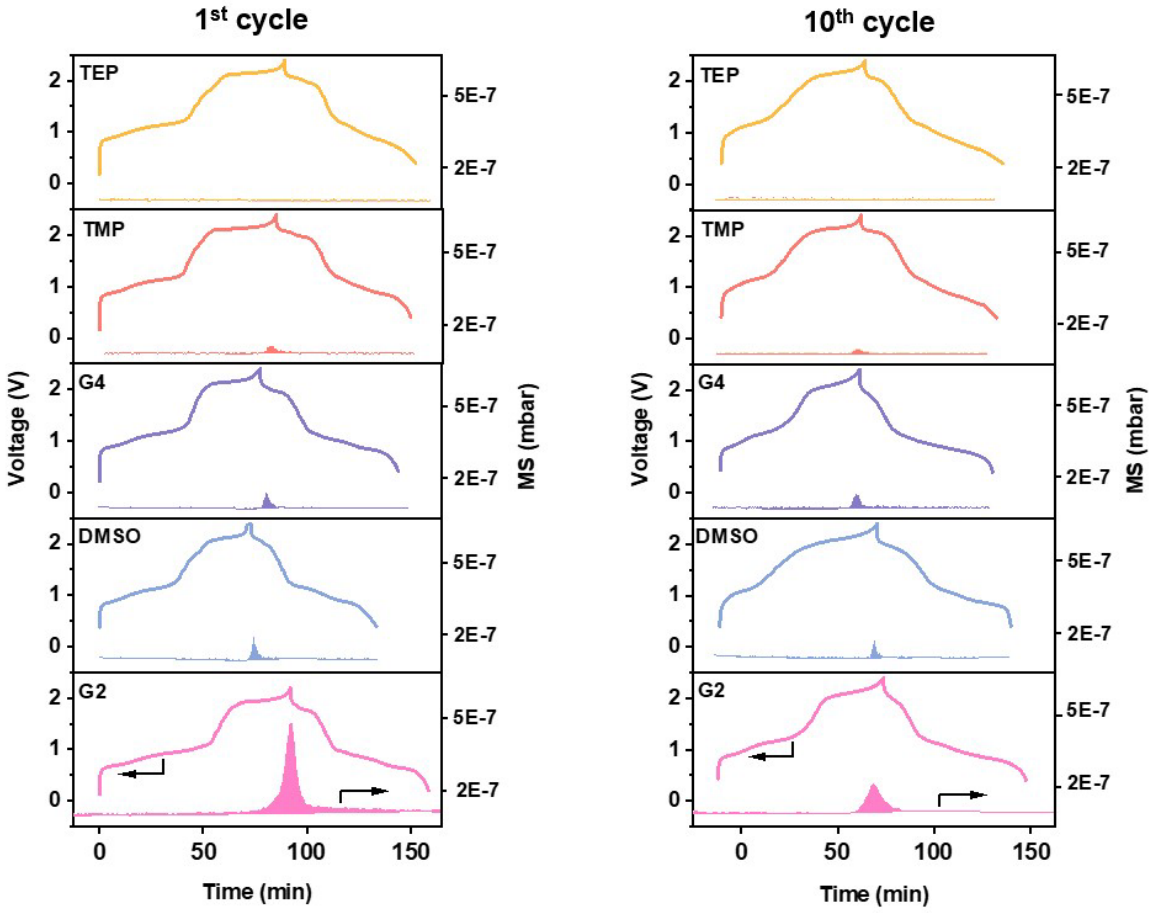

Figure S3. Hydrogen evolution signals in the first and 10th cycles for the V_2O_5//LMO full cells using $LiClO_4$-H_2O-4x electrolytes.

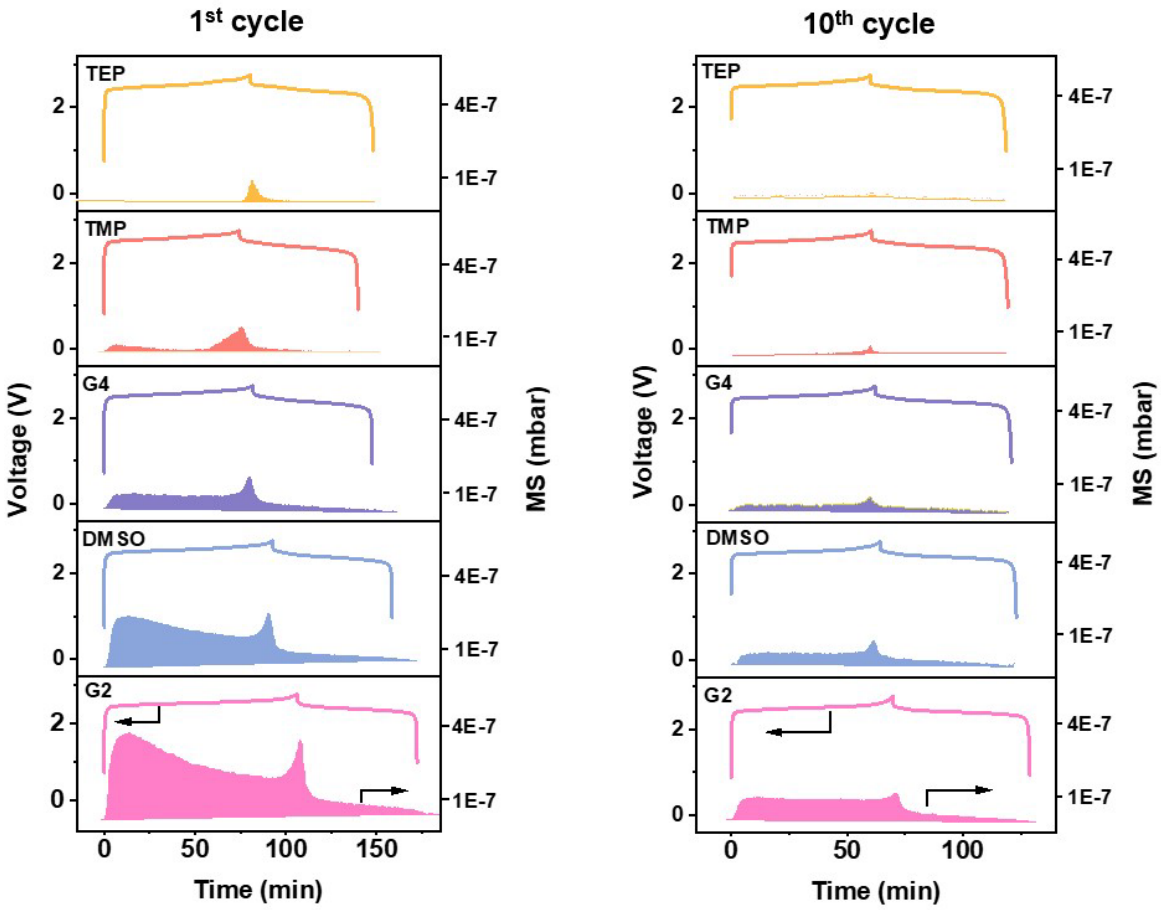

Figure S4. Hydrogen evolution signals in the first and 10th cycles for the LTO//LMO full cells using $LiClO_4$-H_2O-4x electrolytes.

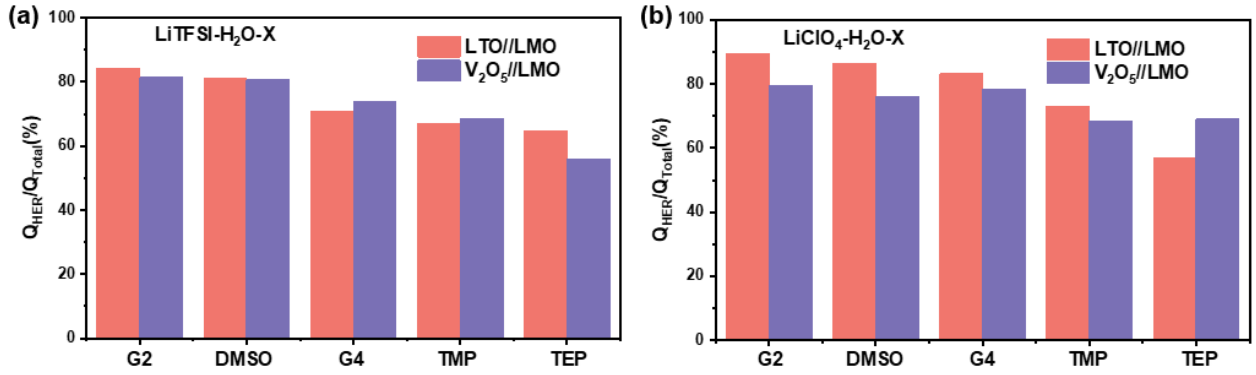

Figure S5. The percentage of the HER-caused irreversible capacity in the total irreversible capacity for 10th cycle of the full cells using (a) LiTFSI-H_2O-x and (b) $LiClO_4$-H_2O-x electrolytes.

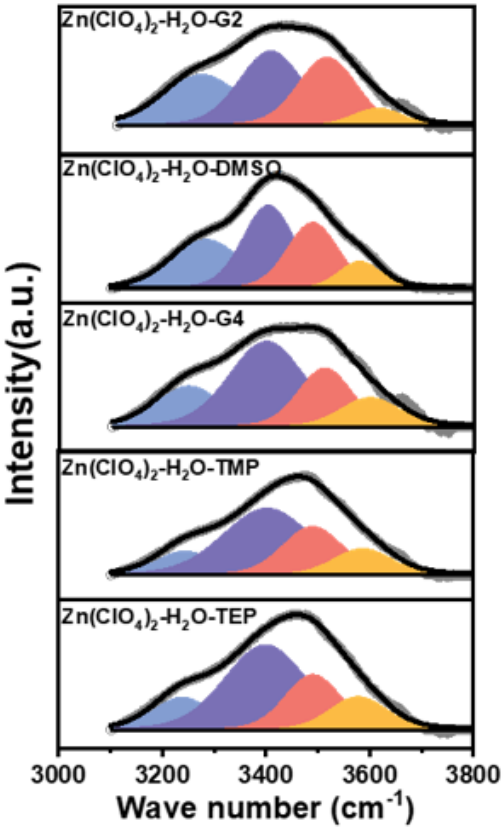

Figure S6. Quantitative analysis of infrared O-H stretching peaks in the $Zn(ClO_4)_2$-H_2O-x electrolytes.

Table S1. The contributions of ICE_{total} and ICE_{HER} (%) in hybrid electrolytes with different I_{A-D} organic modulators.

$LiClO_4$-H_2O-x								
I_{A-D}	LTO//LMO				V_2O_5//LMO			
	1^{st} ICE_{total}	1^{st} ICE_{HER}	10^{st} ICE_{Total}	10^{st} ICE_{HER}	1^{st} ICE_{total}	1^{st} ICE_{HER}	10^{st} ICEtotal	10^{st} ICE_{HER}
58.5	35.49	27.05	10.57	9.47	18.37	10.98	3.68	2.93
59.6	25.1	16.81	7.69	6.65	14.58	7.86	2.86	2.18
83	20.33	12.34	5.27	4.39	12.42	6.48	2.22	1.74
115	16.19	6.35	3.43	2.51	9.32	4.26	1.78	1.22
117	18.26	5.66	2.59	1.47	10.7	3.63	1.52	1.05

LiTFSI-H_2O-x								
I_{A-D}	LTO//LMO				V_2O_5//LMO			
	1^{st} ICE_{total}	1^{st} ICE_{HER}	10^{st} ICE_{Total}	10^{st} ICE_{HER}	1^{st} ICE_{total}	1^{st} ICE_{HER}	10^{st} ICEtotal	10^{st} ICE_{HER}
58.5	20.34	11.52	4.86	4.1	19.23	9.58	2.95	2.4
59.6	15.67	7.51	3.75	3.05	15.14	7.21	2.02	1.63
83	12.19	6.05	3.05	2.16	12.95	4.3	1.57	1.16
115	9.33	4.2	2.16	1.45	10.84	2.85	1.24	0.85
117	10.62	3.35	1.95	1.26	11.38	2.06	0.95	0.53